Proceedings of the International Conference on Oxide Materials for Electronic Engineering (OMEE 2021)

Hydrothermal Synthesis, Structure, and Luminescence of Cr^{3+}-Doped Li_2SnO_3 and Na_2SnO_3 Stannates

L. Vasylechko[a,*], V. Sydorchuk[b], V. Hreb[a], S. Ubizskii[a], S. Khalameida[b], A. Luchechko[c] and Y. Zhydachevskyy[a,d]

[a] *Lviv Polytechnic National University, Bandera Str. 12, 79013 Lviv, Ukraine*
[b] *Institute for Sorption and Problems of Endoecology, NAS of Ukraine, Henerala Naumova Str. 13, 03164 Kyiv, Uraine*
[c] *Ivan Franko National University of Lviv, Universytetska Str., 1, 79000 Lviv, Ukraine*
[d] *Institute of Physics, Polish Academy of Sciences, Aleja Lotnikow 32/46, PL-02668 Warsaw, Poland*

Doi: 10.12693/APhysPolA.141.241 *e-mail: leonid.o.vasylechko@lpnu.ua

Chromium-doped Li_2SnO_3 and Na_2SnO_3 nanocrystalline materials with honeycomb layered monoclinic structure were synthesized by heat treatment of hydrothermally derived precursors at 800 and 900°C, respectively. Evolution of phase composition, structural parameters, and average grain size of the Li_2SnO_3:Cr and Na_2SnO_3:Cr series versus heat treatment temperature were evaluated by full profile Rietveld refinement. The observed structural behaviour reflects complex processes of rearrangement of stacking faults of honeycomb Li_2SnO_3:Cr structure during thermal annealing processes. A deep-red emitting Li_2SnO_3:Cr^{3+} phosphor was obtained and reported for the first time. The ions of Cr^{3+} in Li_2SnO_3 are in the intermediate octahedral crystal field ($Dq/B = 2.48$), which is evident in the photoluminescence occurring at room temperature as broadband stretching from 650 to more than 850 nm ($^4T_2 \rightarrow {}^4A_2$ transitions) with a residual narrow and sharp emission line at 700 nm ($^2E \rightarrow {}^4A_2$). No photoluminescence of Cr^{3+} ions was detected at room temperature in as-prepared Na_2SnO_3:Cr and Li_8SnO_6:Cr materials.

topics: lithium and sodium stannates, hydrothermal synthesis, crystal structure, red luminescence

1. Introduction

Lithium and sodium stannates are of research interest due to their application in lithium-ion batteries and matrices for the preparation of luminescent materials [1–5]. The crystal structure of these stannates is essential for their successful application. It is formed during synthesis and the next treatments. High-temperature solid state and sol-gel techniques using complex reaction mixtures have been described previously in the literature for stannates preparation [2, 4]. Among the existing methods of synthesis, the hydrothermal method is distinguished by the possibility of the formation of crystalline phases at the lowest temperature. Thus, hydrothermal treatment (HTT) reduces temperature to 180–250°C and simplifies the process due to the formation of hydroxostannates, which are precursors of stannates [6]. It also allows using oxides and hydroxides as reagents instead of salts, making it possible to eliminate the stage of washing the products. Therefore, the main tasks of the work were to study the hydrothermal synthesis of chromium-doped lithium and sodium stannates, the evolution of their crystal structure during subsequent calcination, and test their luminescence properties.

2. Experimental

2.1. Samples preparation

For the synthesis of lithium and sodium stannates Li_2SnO_3 and Na_2SnO_3 doped with 0.005 mol% of chromium, we used a wet gel of SnO_2 as a tin source, which promotes maximum homogenization of the reaction mixture in order to ensure maximum contact of the components in the hydrothermal process and a reduction in its duration. A similar approach was used, for example, in the synthesis of barium stannate [7]. The wet gel of SnO_2 with a humidity of 72% was prepared via precipitation from $SnCl_4 \cdot 5H_2O$ solution as described in [8]. The second component was added to the reaction

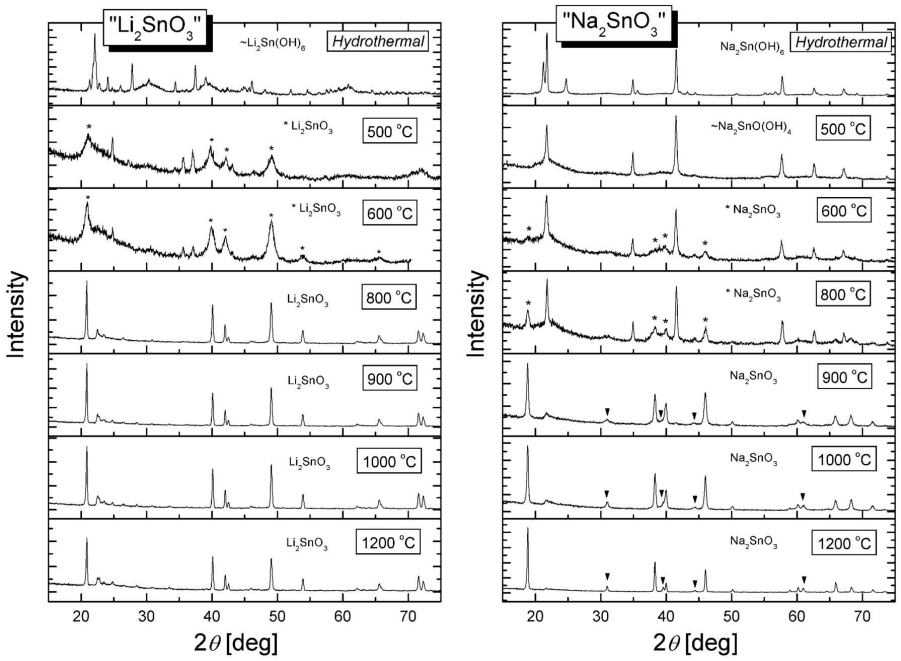

Fig. 1. Evolution of XRD patterns (Co K_α radiation) vs heat treatment temperature of hydrothermal precursors for the synthesis of lithium and sodium stannates. Arrows in (b) indicate SnO_2 secondary phase.

mixture as hydroxides ($LiOH{\cdot}H_2O$ and NaOH) in quantities providing stoichiometric ratios for obtaining Li_2SnO_3 and Na_2SnO_3 stannates. The temperature and duration of the hydrothermal treatment of precursors were 250°C and 5 h. The prepared products were dried in air at 100°C for 5 h and calcined stepwise in the temperature range of 250–1200°C to obtain desired Li_2SnO_3:Cr and Na_2SnO_3:Cr materials.

We also tried to obtain in a similar way lithium-richest stannate Li_8SnO_6 with the rhombohedral crystal structure. However, our attempt was rather unsuccessful — the amount of the desired phase did not exceed 40–50 wt.% in the products heat-treated at 900 and 1000°C, and further annealing at 1200°C led to complete decomposition of Li_8SnO_6 into Li_2SnO_3 and Li_2O.

2.2. Physical-chemical characterization

The differential thermal analysis-thermogravimetric (DTA-TG) curves were recorded in air using the Derivatograph-apparatus (Paulik–Paulik–Erdey system, MOM, Hungary) in the temperature range of 20–1000°C at the heating rate of 10°C/min. The phase composition of crystal structure was monitored at all stages of the synthesis procedure using a modified DRON-3M X-ray powder diffractometer. Crystal structure parameters were derived from experimental X-ray diffraction (XRD) data by the full profile Rietveld refinement using the WinCSD program package [9]. The latter was also applied to evaluate the average crystalline size (D_{ave}) and microstrains ($\langle\varepsilon\rangle$) values from angular dependence of diffraction maxima profiles.

2.3. Photoluminescence characterization

Photoluminescence (PL) and photoluminescence excitation (PLE) spectra were measured using a Horiba/Jobin-Yvon Fluorolog-3 spectrofluorometer with a 450 W continuous spectrum xenon lamp for excitation and optical detection, with a Hamamatsu R928P photomultiplier operating in the photon counting mode. The measured PLE spectra were corrected with the xenon lamp emission spectrum. The PL spectra were corrected for the spectral response of the spectrometer system used.

3. Results and discussion

XRD examinations of as-obtained products after hydrothermal treatment revealed the formation of different forms of lithium and sodium hydroxostannates directly in hydrothermal reactions (Fig. 1, upper rows). Rhombohedral crystal structure of $Na_2Sn(OH)_6$ was further confirmed by full profile Rietveld refinement.

Subsequent heat treatment of the products at 500 and 600°C for 2 h lead to gradual decomposition of the hydroxostannates and the beginning of the formation of anhydrous Li_2SnO_3 and Na_2SnO_3. This was proved by both XRD (Fig. 1) and DTA-TG (Fig. 2) data, which revealed a significant mass loss in the temperature range of 250–500°C, similar as for other hydroxostannates prepared under hydrothermal conditions [6, 7].

Phase pure Li_2SnO_3:Cr material is formed after heat treatment of the product at 800°C. Further heat treatment at 900, 1000, and 1200°C does not affect the phase composition. Only narrowing of

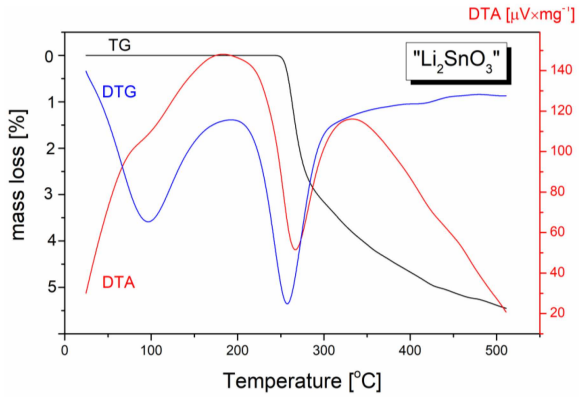

Fig. 2. DTA-TG-DTG curves of hydrothermal precursors for the synthesis of Li_2SnO_3.

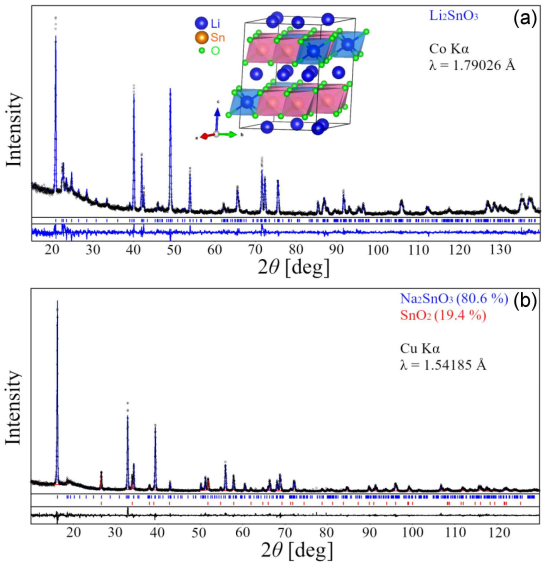

Fig. 3. Graphical results of the Rietveld refinement of Li_2SnO_3 (a) and Na_2SnO_3 (b) structures. X-ray powder diffraction patterns (black dots) are shown in comparison with calculated ones (blue and red lines). Inset in (a) shows view of Li_2SnO_3 two-layer structure.

diffraction peaks is observed due to improving the degree of crystallinity of the material (see Fig. 1). The average grain size D_{ave} of Li_2SnO_3:Cr powders increases sharply from 7–9 nm after its formation at 500–600°C up to 175–280 nm after additional heat treatment at 800°C and higher temperatures. Simultaneously, a sharp reduction of the average microstrains values $\langle\varepsilon\rangle$ associated with the dispersion of interatomic distances is observed in the same temperature range.

Another phase and structural behaviour are observed in the case of the hydrothermal precursor of Na_2SnO_3 (see Fig. 1b). As mentioned above, the pure phase of sodium hydroxostannate is formed immediately after HTT, which partially decomposes to form an intermediate product of dehydration after annealing at 500°C. Reflexes of the desired phase Na_2SnO_3 begin to appear after the next annealing of the powders at 600°C, and it becomes the dominant phase after the subsequent heat treatment of samples at 900°C. Besides the main Na_2SnO_3, a detectable amount of tetragonal SnO_2 cassiterite phase (PDF-2 card N 41-1445) could be observed in the powders annealed at 900, 1000, and 1200°C (Fig. 1b).

Precise structural parameters of both Li_2SnO_3:Cr and Na_2SnO_3:Cr series annealed at different temperatures were evaluated from experimental XRD patterns by the full profile Rietveld refinement (see Fig. 3). As the starting models for the refinement, the atomic coordinates in Li_2SnO_3 and Na_2SnO_3 structures derived from neutron diffraction data in [10] and [11] were used. For the Na_2SnO_3:Cr materials containing admixtures of SnO_2 oxide, simultaneous two-phase Rietveld refinement was performed. It is worth noting that the experimental XRD pattern of Li_2SnO_3:Cr material show rather sharp superstructure reflections in 2θ range of 21–38° (Co K_α) arising from honeycomb ordering in $LiSn_2$ slabs of Li_2SnO_3 structure. These superstructure reflections could be satisfactorily fitted only assuming mixed occupancy of two 4e octahedral sites occupied with Li and Sn cations (see Table I). In the case of Na_2SnO_3:Cr, the superstructure reflections are much less pronounced. However, to properly model the (020) peak at $2\theta \approx 18.6°$ (Cu K_α), the mixed occupancy of three 4e and one 4d fourfold sites with Na and Sn cations are required (Table II). Note that the mixed occupancy of some octahedral positions in both Li_2SnO_3:Cr and Na_2SnO_3:Cr structures are rather apparent, and reflect stacking fault in such kinds of honeycomb structures, as it was recently reported [5, 11].

Graphical results of the Rietveld refinement of Li_2SnO_3:Cr^{3+} and Na_2SnO_3:Cr^{3+} structures and appropriate parameters obtained are presented in Fig. 3 and Tables I and II, respectively.

In the monoclinic $C2/c$ Li_2SnO_3 structure, there are three nonequivalent octahedral positions of Li^+ ions and two octahedral sites of Sn species (Table I). Accordingly, there are three different kinds of distorted [LiO_6] octahedra around Li1, Li2, and Li3 atoms with the average Li–O distances of 2.258, 2.153, and 2.147 Å, respectively, and two kinds of [SnO_6] octahedra with Sn1–O and Sn2–O average distances of 2.117 Å and 2.043 Å, respectively. These values of interatomic distances, calculated from the atomic coordinates in the Li_2SnO_3:Cr^{3+} structure presented in Table I, are in good agreement with the average Li–O and Sn–O distances of 2.202 and 2.069 Å derived from neutron diffraction data for Li_2SnO_3 in [10]. Octahedral coordination of Sn atoms in Li_2SnO_3structure offers a good chance to accept Cr^{3+} ions, due to similar ionic radii of Sn^{4+} and Cr^{3+} ions (0.69 and 0.615 Å)

TABLE I

Lattice parameters, coordinates, and displacement parameters of atoms in Li_2SnO_3:Cr^{3+} structure after heat treatment at 1200°C (SG $C2/c$, $Z = 4$). Lattice parameters: $a = 5.2949(2)$ Å, $b = 9.1850(4)$ Å, $c = 10.0232(2)$ Å, $\beta = 100.280(3)°$, $V = 479.64(5)$ Å^3; residuals: $R_I = 0.061$, $R_P = 0.218$.

Atoms, sites	x/a	y/b	z/c	$B_{iso/eq}$ [Å^2]
Sn1*, 4e	0	0.4132(5)	1/4	0.70(5)
Sn2, 4e	0	0.7463(4)	1/4	0.83(5)
O1, 8f	0.142(4)	0.246(2)	0.138(2)	0.7(4)
O2, 8f	0.136(4)	0.594(2)	0.1388(12)	0.4(3)
O3, 8f	0.148(4)	0.900(2)	0.129(2)	2.7(4)
Li1, 8f	0.228(9)	0.066(6)	0.012(4)	1.3(8)
Li2, 4d	1/4	1/4	1/2	1.0(12)
Li3*, 4e	0	0.068(2)	1/4	0.6(3)

*Sn1 = 0.876(7) Sn + 0.124(7) Li,
Li3 = 0.854(4) Li + 0.146(4) Sn

TABLE II

Lattice parameters, coordinates and displacement parameters of atoms in Na_2SnO_3:Cr^{3+} structure after heat treatment at 1200°C (SG $C2/c$, $Z = 4$). Lattice parameters: $a = 5.5186(4)$ Å, $b = 9.5695(9)$ Å, $c = 11.0673(1)$ Å, $\beta = 99.55(1)°$, $V = 576.4(1)$ Å^3; residuals: $R_I = 0.064$, $R_P = 0.210$.

Atoms, sites	x/a	y/b	z/c	$B_{iso/eq}$ [Å^2]
Sn1*, 4e	0	0.4093(7)	1/4	0.68(11)
Sn2*, 4e	0	0.7427(7)	1/4	0.75(10)
O1, 8f	0.152(9)	0.256(5)	0.1275(15)	1.6(7)
O2, 8f	0.141(10)	0.591(4)	0.150(2)	0.4(6)
O3, 8f	0.114(10)	0.897(4)	0.153(2)	1.0(7)
Na1, 8f	0.226(4)	0.060(2)	0.0014(14)	0.8(3)
Na2*, 4d	1/4	1/4	1/2	0.5(4)
Na3*, 4e	0	0.089(2)	1/4	0.5(2)

*Sn1 = 0.81(2) Sn + 0.19(2) Na,
Sn2 = 0.95(2) Sn + 0.05(2) Na,
Na2 = 0.936(8) Na + 0.064(8) Sn,
Na3 = 0.766(10) Na + 0.234(10) Sn

after Shannon [12]. The linked Li- and Sn-occupied octahedra in Li_2SnO_3 structure form two types of layers, one composed of [LiO_6] only and the other composed of [LiO_6] and [SnO_6] octahedra in the ratio 1:2, stacked alternately along the c-axis [10]. The cations of the mixed layers are ordered in such a way that they form hexagonal close-packed planes in which Sn atoms occupy the vertices of the hexagons, and the Li atoms are placed in their centers [10].

Analysis of structural parameters of Li_2SnO_3:Cr series annealed at different temperatures revealed that increase of heat treatment temperature affects in the opposite way the lattice parameters of the materials — a sharp decrease of the a-parameter between 800 and 900°C is accompanied by a simultaneous increase in the b- and c-parameters and monoclinic angle β (Fig. 4). It is evident that the observed deviations reflect the complex processes of rearrangement of stacking faults of the honeycomb structure and possible redistribution of cations in the Li_2SnO_3:Cr structure.

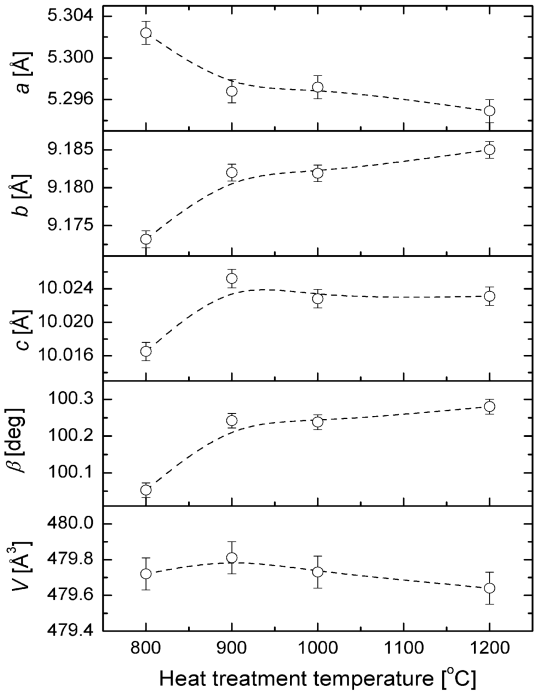

Fig. 4. Evolution of the lattice parameters, monoclinic angle, and unit cell volume of Li_2SnO_3:Cr series vs heat treatment temperature of the powders. Dashed lines are B-spline approximations for a guide for eyes.

Typical photoluminescence excitation and emission spectra of Li_2SnO_3:Cr calcined at 1200°C are shown in Fig. 5. The emission spectrum of this phosphor reveals broadband stretching from about 650 to more than 850 nm with a superimposed narrow line at 700 nm, which can be attributed to the $^4T_2 \rightarrow {}^4A_2$ and $^2E \rightarrow {}^4A_2$ radiative transitions in Cr^{3+} ion, respectively [13]. The photoluminescence decay time of 0.1 ms, measured for the narrow line at room temperature, suggests that the ^2E level is strongly thermalized by the $^4T_2$ level at room temperature. The excitation spectrum (regardless of the emission wavelength) represents two broadbands with maxima at about 440 and 617 nm, which are associated with the $^4A_2 \rightarrow {}^4T_1$ and $^4A_2 \rightarrow {}^4T_2$ transitions in Cr^{3+} ions, respectively. The third excitation band at about 260 nm (see Fig. 6a) most probably is associated with a charge-transfer transition related to Cr^{3+}. When the emission is registered far in the deep-red, a narrow and sharp line at 700 nm related to the ^2E level can also be revealed in the excitation.

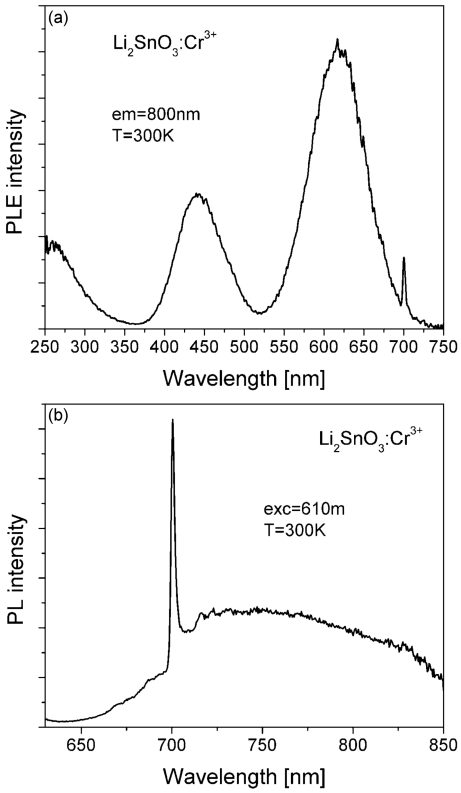

Fig. 5. Room-temperature photoluminescence excitation (a) and photoluminescence emission (b) spectra of Li_2SnO_3:0.0005%Cr phosphor.

A simultaneous presence of the broad and the narrow emission bands in Li_2SnO_3:Cr suggests that Cr^{3+} ions occupying the Sn-octahedral positions in this host are affected by an intermediate crystal field strength producing a close energy position of the $^4T_2$ and ^2E levels, similarly as in β-Ga_2O_3:Cr^{3+} [13, 14] or $La_3Ga_5SiO_{14}$:Cr^{3+} [15]. Taking the $^4A_2 \rightarrow {}^4T_1$ and $^4A_2 \rightarrow {}^4T_2$ peak positions as 440 and 617 nm, respectively, one can estimate the crystal field strength parameter $Dq/B = 2.48$. At the same time, the narrow line related with the $^2E \rightarrow {}^4A_2$ transition, which is observed as a single non-resolvable line (at least at room temperature), suggests that a CrO_6 octahedron in Li_2SnO_3 is much more regular than in other oxide compounds like Ga_2O_3, Al_2O_3 or even $Y_3Al_5O_{12}$ (see [16], for instance). In order to reveal more features of the Cr^{3+} luminescence in Li_2SnO_3, detailed temperature-dependent studies should be done.

As regards the Na_2SnO_3:Cr and Li_8SnO_6:Cr materials, no photoluminescence that could be attributed to Cr^{3+} ions was detected at room temperature.

4. Conclusions

Chromium-doped Li_2SnO_3 and Na_2SnO_3 nanocrystalline materials with honeycomb layered monoclinic structure were synthesized by hydrothermal route from a wet gel of SnO_2 and hydroxides $LiOH{\cdot}H_2O$ and NaOH as tin and alkali-metal sources, respectively. In the case of Li_8SnO_6:Cr materials, the amount of the desired phase does not exceed 40–50 wt.% in the best final product. Structural parameters of as-obtained Li_2SnO_3:Cr and Na_2SnO_3:Cr materials, derived from X-ray powder diffraction data in our study, are in good agreement with the reported parameters for the parent compounds elucidated from neutron powder diffraction. Observed nonuniform behaviour of structure parameters in Li_2SnO_3:Cr with increasing heat treatment temperature (sharp decrease of the a-parameter and simultaneous increase of the b- and c-parameters and monoclinic angle) evidently reflects complex processes of rearranging the stacking faults of honeycomb Li_2SnO_3:Cr structure during thermal annealing.

It was found that Cr^{3+} ions in the Li_2SnO_3 lattice are affected by an intermediate octahedral crystal field ($Dq/B = 2.48$) and give a deep-red broadband at room temperature due to the $^4T_2 \rightarrow {}^4A_2$ transitions, simultaneously with a residual narrow line due to the $^2E \rightarrow {}^4A_2$ transition, with the decay time 0.1 ms at room temperature. The excitation bands maxima associated with the $^4A_2 \rightarrow {}^4T_2$ and $^4A_2 \rightarrow {}^4T_1$ electronic transitions are at 617 and 440 nm, respectively. In such a way, this study provides a new interesting structurally stable Cr^{3+}-doped deep-red emitting phosphor.

Acknowledgments

The work was funded by the National Research Foundation of Ukraine under grant no. 2020.02/0373 "Crystalline phosphors' engineering for biomedical applications, energy saving lighting and contactless thermometry". Y.Z. acknowledges support of the Polish National Science Centre (project no. 2018/31/B/ST8/00774).

References

[1] N. Musa, H.J. Woo, L.P. Teo, A.K. Arof, *Mater. Today Proc.* **4**, 5169 (2017).

[2] Y. Zhao, X. Li, B. Yan, D. Xiong, D. Li, S. Lawes, X. Sun, *Adv. Energy Mater.* **6**, 1502175 (2016).

[3] M. García-Tecedor, J. Bartolomé, D. Maestre, A. Trampert, A. Cremades, *Nano Res.* **12**, 441 (2019).

[4] R. Cao, W. Wang, J. Zhang, S. Jiang, Z. Chen, W. Li, X. Yu, *J. Alloys Compd.* **704**, 124 (2017).

[5] F. Lu, W. Zeng, H. Lin, S. Liu, X. Tian, J. Yang, J. Li, Y. Yang, *Electrochim. Acta* **315**, 48 (2019).

[6] Y. Zhao, Y. Huang, Q. Wang, X. Wang, M. Zong, *Ceram. Int.* **39**, 1741 (2013).

[7] W. Lu, H. Schmidt, *J. Eur. Ceram. Soc.* **25**, 919 (2005).

[8] S.V. Khalameida, M.N. Samsonenko, V.V. Sydorchuk, V.L. Starchevskyy, O.I. Zakutevskyy, O.Yu. Khyzhun, *Theor. Exp. Chem.* **53**, 40 (2017).

[9] L. Akselrud, Y. Grin, *J. Appl. Crystallogr.* **47**, 803 (2014).

[10] J.L. Hodeau, M. Marezio, A. Santoro, R.S. Roth, *J. Solid State Chem.* **45**, 170 (1982).

[11] R.W. Smaha, J.H. Roudebush, J.T. Herb, E.M. Seibel, J.W. Krizan, G.M. Fox, Q. Huang, C.B. Arnold, R.J. Cava, *Inorg. Chem.* **54**, 7985 (2015).

[12] R.D. Shannon, *Acta Crystallogr. A* **32**, 751 (1976).

[13] S. Adachi, *ECS J. Solid State Sci. Technol.* **9**, 026003 (2020).

[14] A. Luchechko, V. Vasyltsiv, Y. Zhydachevskyy, M. Kushlyk, S. Ubizskii, A. Suchocki, *J. Phys. D Appl. Phys.* **53**, 354001 (2020).

[15] M. Casalboni, A. Luci, U.M. Grassano, B.V. Mill, A.A. Kaminskii, *Phys. Rev. B* **49**, 3781 (1994).

[16] V. Mykhaylyk, H. Kraus, Y. Zhydachevskyy, V. Tsiumra, A. Luchechko, A. Wagner, A. Suchocki, *Sensors* **20**, 5259 (2020).